Dynamic Effects on Migratory Aptitudes in Carbocation Reactions

Zhitao Feng and Dean J. Tantillo*

Department of Chemistry, University of California, Davis, One Shields Avenue, Davis, California 95616, United States

ABSTRACT: Carbocation rearrangement reactions are of great significance to synthetic and biosynthetic chemistry. In pursuit of a scale of inherent migratory aptitude that takes into account dynamic effects, both uphill and downhill *ab initio* molecular dynamics (AIMD) simulations were used to examine competing migration events in a model system designed to remove steric and electronic biases. The results of these simulations were combined with detailed investigations of potential energy surface topography and variational transition state theory calculations to reveal the importance of non-statistical dynamic effects on migratory aptitude.

1.Introduction

One could argue that the field of carbocation rearrangement reactions was birthed in 1859 when Fittig treated pinacol with sulfuric acid and discovered the pinacol rearrangement.[1] Since then, carbocation rearrangements have been shown to play critical roles in biological,[2] synthetic,[3] and physical organic chemistry,[4] both because of the efficiency by which such rearrangements can be used to construct complex polycyclic systems and because they have served as testing grounds for non-traditional bonding and mechanistic concepts such as three-center two-electron bonding,[5] flat potential energy surfaces (PESs) in which expected intermediates are not minima,[6] anchimeric assistance,[7] post-transition state bifurcations (PTSB),[4] and non-statistical dynamic effects (including memory effects).[8] In most cases, it is theoretically possible for more than one group to migrate to a given carbocation center during rearrangement. The tendency of a group to migrate, its "migratory aptitude", depends both on the inherent properties of the group and on context. The latter is related to, for example, what type of carbocation will be formed upon migration (e.g., tertiary vs. secondary) and the orientation of the migrating group relative to the formally empty p-orbital on the carbocation (carbenium ion) center (e.g., hyperconjugated or not). Here we focus on the former, especially the dynamic behavior of the migrating group, in pursuit of a new scale of "migratory aptitude that accounts for dynamic effects".

Much work has been done in the field of carbocation migratory aptitudes over the past few decades, from both experimental and theoretical perspectives. Experimental efforts focused on measuring rates for various simple rearrangements and comparing yields between different migrations.[9] For instance, Vogel and co-workers demonstrated the high migratory tendency of acyl groups in multiple synthetically relevant scenarios.[10] Frontier and co-workers examined the balance between electronic effects and steric hindrance in their examination of sequential Narazov electrocyclization/Wagner-Meerwein rearrangement reactions.[11] These are but two examples that showcase the relevance of the migratory aptitude concept to synthetic organic chemistry.

Early theoretical work utilized density functional theory (DFT) to locate transition state structures (TSSs) and compare their energies to predict migratory aptitudes.[12] More recently, molecular dynamics (MD) simulations by Riveros, Longo and co-workers were used to probe non-statistical dynamic effects on migratory aptitudes associated with the absence of minima corresponding to secondary carbocations.[4,6,13] These two examples highlight the two common types of approaches — static and dynamic — employed in computational studies on carbocation rearrangement reactions.

While it is well-known that various factors contribute to the magnitudes of migratory aptitudes, a common rule of thumb for estimating migratory aptitude is: groups that better stabilize a carbocation will migrate preferentially. This guideline captures, to some degree, the fact that positive charge generally builds up on a group during migration to a carbocation center. But there are notable exceptions to this rule of thumb. For example, in some cases less substituted CR_2 groups have been shown to migrate preferentially over more substituted CR_2 groups, even when significant differences between the stability of resulting carbocations are not apparent.[14] Also, H atoms can display a high migratory tendency.[11,15] Recent work also has shown that the inherent properties of the migrating group can be overwhemed by the properties of the framework over which migration occurs.[15b] Here we revisit the concept of migratory aptitude in pursuit of a theoretical framework that provides both fundamental understanding and principles that are useful for synthesis design.

Inspired by the pinacol rearrangement,[1,16] which has served as a useful platform for evaluating migratory aptitudes in the past and for which previous simulations indicate the importance of non-statistical dynamic effects,[17,18] we designed the model system shown in Scheme 1. In this system, both R^1 and R^2 are oriented similarly with respect to the leaving group and carbocation center formed upon its departure, so that conformational issues are avoided. Migration of either R^1 or R^2 will lead to a benzylic cation so that product stability issues are minimized. The group that migrates moves towards the non-migrating group, which should minimize differences in

steric congestion as one or the other group migrates. In short, this system was designed to minimize context effects so that inherent migratory aptitudes can be exposed. In addition, the leaving group chosen here was water, rather than an anionic leaving group, to minimize charge separation during reaction and associated complications.[7] This system was also designed such that initial leaving group loss would lead to a secondary carbocation expected not to be a minimum on the PES,[4,6,13] which would lead to a PTSB,[19] i.e., there would be a single ambimodal[20] TSS followed by pathways downhill in energy to the products of migration of R^1 and R^2, thereby forcing migratory preferences to be controlled by non-statistical dynamic effects. While our results bear out the expectation that the secondary cation is not a minimum, separate TSSs for concerted (but asynchronous) water loss and migration were found for R^1 and R^2; this scenario complicated our analysis but also introduced an opportunity to examine additional aspects of migratory behavior.

We applied several computational approaches and reactivity models to characterize behavior during migration. Our main approach involved uphill *ab initio* molecular dynamics (AIMD) simulations,[4c,15j,21] in which additional momenta were added to reactants to promote water loss. The validity of such an approach is supported by comparisons with experimental product distributions (*vide infra*). The relative abundance of trajectories for migration of R^1 and R^2 provides a measure of migratory ability. We compared these predictions to predictions arrived at by comparing free energies of TSSs on PESs[22] and by comparing free energies of variational transition states (VTSs).[23] Intrinsic reaction coordinates (IRCs)[24] and models of PESs, as well as the results of downhill AIMD simulations (initiated from VTSs) were also explored; these pointed to potential roles of recrossing and pathway bifurcations. We arrived at a ranking of migratory aptitudes and a model in which this ordering is rationalized based on dynamic effects. Ultimately, we tested our methods on a real-world synthetic example and these not only revealed non-statistical dynamic effects, but also accurately predicted the product ratio observed in the experiment (where other methods and models did not).[25]

Scheme 1. Model reaction for comparing migratory aptitudes of R^1 and R^2.

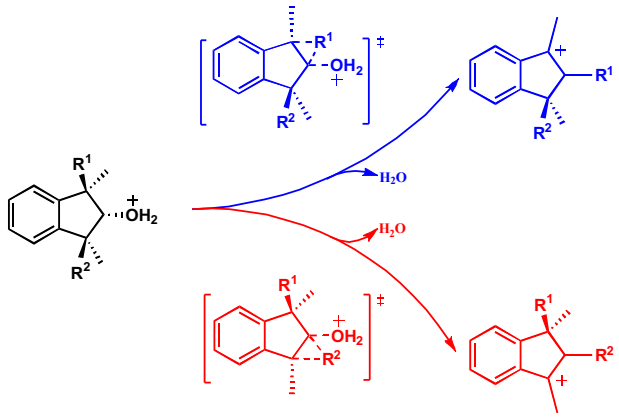

2. Computational Methods

Geometry optimizations and frequency calculations were carried out with the *Gaussian16* C.01 package[26] at the M06-2X-D3/6-31G(d)[27] level of theory (see Supporting Information Table S1 for results of tests with more levels of theory). DLPNO-CCSD(T)[28] calculations were performed with ORCA 4.2.1.[29] PES minima and TSSs were identified by the number of imaginary frequencies obtained in frequency calculations, with 0 for minima and 1 for TSSs. VTSs and free energy reaction coordinates were calculated with *Gaussrate/Polyrate*.[29] Quasi-classical AIMD simulations from reactants and VTSs were performed using the *Progdyn* script with a temperature of 298 K in the NVE ensemble.[31] The vibrational modes and forces were calculated quantum mechanically while the trajectories were propagated classically using the velocity Verlet algorithm with a timestep of 1 fs.[32] For uphill dynamics, breaking of the C–O bond was promoted by adding energy to the momentum vectors that have the direction of elongating the C–O bond, i.e., we only examine trajectories associated with water loss. Different amounts of excess energy were tested and compared with the experimental results. While the selectivity of migration varies (see Table S2 in Supporting Information and section 3.6 for details), the results indicate that the variation is not large (maximum deviation of less than 10%). Consequently, we used an excess energy of 25.0 ± 0.1 kcal/mol for all systems. The thresholds of C–C and C–H bond formation used to terminate trajectories were 1.6 Å and 1.1 Å, respectively. Due to the rigidity of the molecule and the distance between the migrating groups, the influence of conformational flexibility on uphill dynamic simulations is expected to be small and was not examined exhaustively (see Supporting Information for details). *CYLview* was used for visualization of molecular geometries.[33]

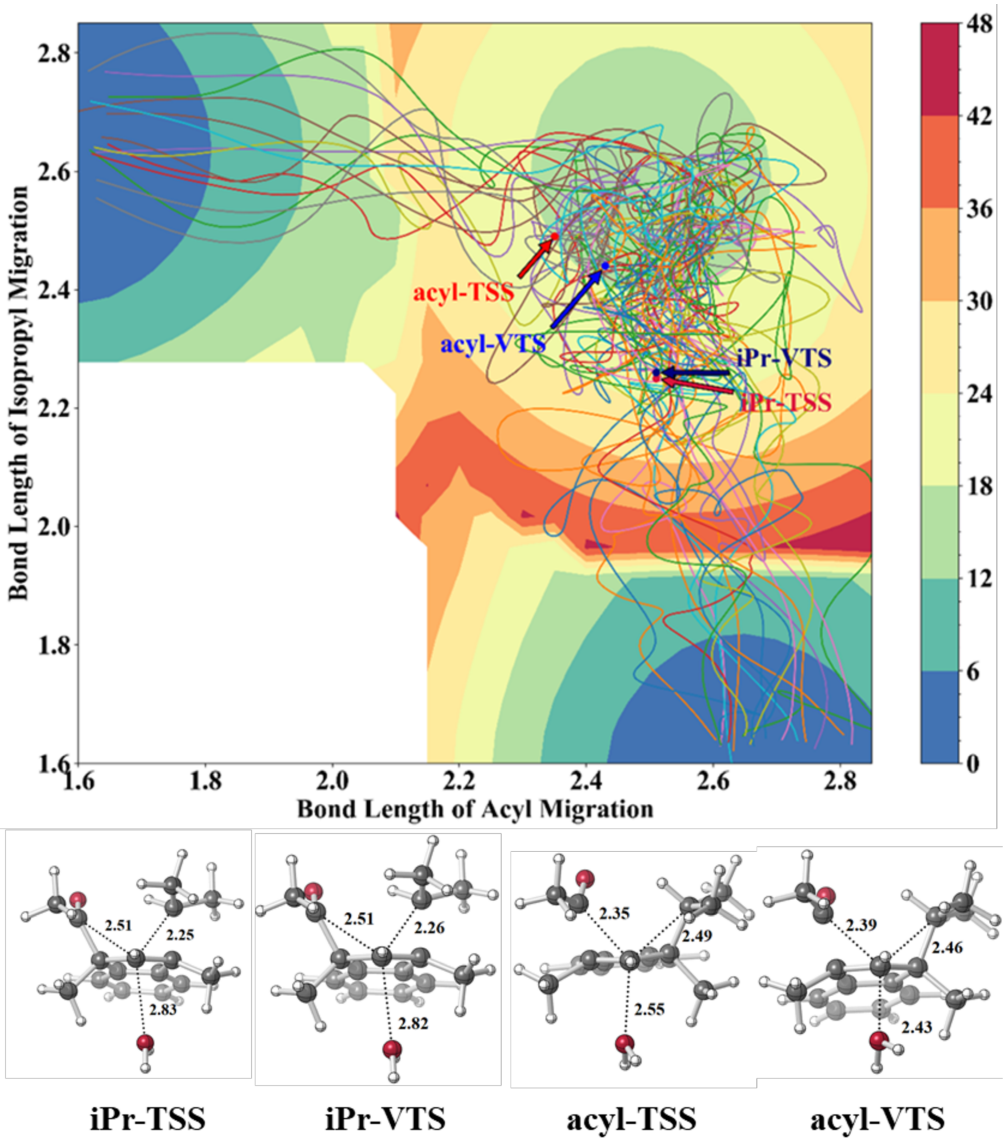

Figure 1. PES with representative trajectories for the R^1 = acyl, R^2 = *i*-Pr system at the M06-2X-D3/6-31G(d) level projected onto it. The axes correspond to the length (Å) of one or the other C–C bond formed upon migration of R^1 or R^2. The valley at the top right corresponds to the reactant region and the valleys at the top left and bottom right correspond to the two product regions. Points corresponding to the bond lengths in both TSSs and VTSs are labeled and the geometries of these structures are shown below the plot.

3. Results & Discussion

3.1 Shape of PES. To provide context for the results of our dynamics simulations, a 2D contour plot of the PES for the secondary carbocation formed for the R^1 = acyl, R^2 = *iso*-propyl system was calculated (Figure 1). The PES was derived by scanning the C^1–R^1 and C^1–R^2 bond lengths while relaxing all other degrees of freedom. The void space at the bottom left of the PES results from the two migrating groups being too close to each other and associated SCF convergence failures. Some regions of discontinuity in energy are also likely the result of the use of only two degrees of freedom. Despite these complications associated with reduced-dimension (much less than 3N-6 dimensions corresponding to all degrees of freedom) PESs,[34] important features are revealed in this plot. The three valleys correspond to the reactant (top right) and two products (top left and bottom right). Points corresponding to the bond lengths in both TSSs (and VTSs, *vide infra*) are labeled. Again, the reduced dimensionality of this PES is partly responsible for these TSSs not residing at points that look like simple first-order saddle points. Uphill trajectories also have been projected onto the PES (curved lines), and these will be discussed below. One noteworthy feature of this PES is that the reactant minimum is surrounded by roughly oval contours that connect the pathways to each of the two products, i.e., the two competing pathways are not separated by a high energy feature in the region between transition states. As a result, leakage between these two pathways is possible, i.e., trajectories initially progressing towards one product may end up in the other by traversing this relatively flat region of the PES. Such a feature implies

that the behavior after passing through the transition state regions cannot be neglected, a scenario for which transition state theory fails to account.[23a] This scenario mandates caution in attempting to make selectivity predictions based on energies of transition states alone.

3.2 Uphill dynamics. Uphill AIMD trajectories were initiated from the reactant for systems with a variety of R^1 and R^2 groups (reasonably representative of those of interest to synthetic chemists; Table 1). The percentage of trajectories leading to each product, along with barriers for formation of each product based on free energies of TSSs (and VTSs for selected systems; see below) are shown in Table 1. Since each system has a built-in competition between two migrating groups, we arrive at an overall, qualitative, ordering of migratory abilities, assuming that the migratory aptitude is transitive. The AIMD results indicate the following order of migratory aptitude: cyclobutyl > vinyl ≈ Ph > CH_2-cyclopropyl ≈ cyclopropyl ≈ *iso*-propyl ≈ acyl > allyl ≈ ethyl > methyl ≈ H > methoxymethyl. While a similar ordering is arrived at using free energies of TSSs, the magnitudes of some preferences vary significantly in AIMD-based and transition state free energy-based predictions, especially with H or acyl groups as migrators.

Table 1. Results of uphill dynamic simulations, conventional and variational free energy barriers and predicted product ratios (M06-2X-D3/6-31G*), energies in kcal/mol).

	R^1				R^2				trajectory-based product ratio	TSS-based product ratio	VTS-based product ratio	Total trajectories
		%	$\Delta G^{\ddagger}_{TSS}$	$\Delta G^{\ddagger}_{VTS}$		%	$\Delta G^{\ddagger}_{TSS}$	$\Delta G^{\ddagger}_{VTS}$				
1	H—R	32%	9.5	9.7	H_3C—R	45%	9.7	9.8	42:58	58:42	54:46	88
2	H—R	44%	9.4			55%	9.1		44:56	38:62		102
3	H—R	29%	9.2	9.3		69%	6.6	7.0	30:70	1:99	2:98	116
4	H—R	26%	8.8	9.1		53%	4.8	4.9	27:73	0:100	0:100	204
5	H—R	9%	9.0	9.1	Ph—R	83%	4.6	4.8	10:90	0:100	0:100	82
6	H_3C—R	79%	9.6	10.2		13%	9.7	10.3	86:14	54:46	54:46	176
7	H_3C—R	27%	8.3			54%	7.8		33:67	29:71		77
8		42%	7.5			36%	7.8		55:45	63:37		123
9		75%	7.8		H_3C—R	11%	8.3		87:13	71:29		119
10		49%	7.0			36%	7.1		58:42	54:46		105
11		59%	5.1	6.7		29%	7.9	7.9	67:33	99:1	89:11	76
12		50%	6.4	7.0		47%	7.1	7.4	53:46	77:23	66:34	72
13		50%	6.2	6.2		50%	5.2	5.5	50:50	16:84	24:76	137
14		39%	6.5	6.5		58%	4.7	5.6	40:60	4:96	17:83	128
15	H_3C—R	26%	7.0	7.0		74%	5.1	5.5	26:74	2:98	8:92	100
16	H_3C—R	24%	7.4			69%	6.5		26:74	19:81		114
17		33%	8.2	8.3		58%	6.5	6.8	36:64	5:95	8:92	143
18		33%	7.4	7.5		50%	5.6	5.8	40:60	4:96	6:94	76
19		34%	6.3			64%	6.4		35:65	54:46		117
20		33%	6.7			59%	6.7		36:64	50:50		123
21		48%	6.7			52%	7.0		48:52	62:38		122
22		41%	4.5			47%	5.7		45:55	88:12		116
23		33%	4.5			67%	3.8		33:67	24:76		213

3.3 Variational transition states. To make sure that differences between predictions based on AIMD and transition state energies were not the result of neglecting variational effects,[23a] canonical VTSs were located for a subset of systems. Compared with predicted product distributions based on conventional TSS free energies, some of those based on VTS free energies are closer to the results of uphill AIMD simulations (Table 1). Still, the VTS-based and AIMD-based predictions often differ substantially. Free energy-based reaction pathways were also computed. Representative pathways, for the R^1 = methyl, R^2 = methoxymethyl system, are shown in Figure 2. The black dashed line at the center indicates where the conventional TSSs are located; the VTSs are earlier than the TSSs, as expected for a fragmentation reaction based on assumptions about entropy. For this system, the geometries of the two VTSs are similar to each other, but skewed slightly toward the geometries of reactants to which they are connected. Several new intermediates (here, resulting from inclusion of ZPE; see SI for details),[35] are revealed along these pathways as well, although these are very shallow (barriers < 0.5 kcal/mol). While some differences between TSSs and VTSs and the pathways connected to them are present, these are not large enough to rationalize the differences in predicted product distributions derived from transition state energies and uphill AIMD simulations.

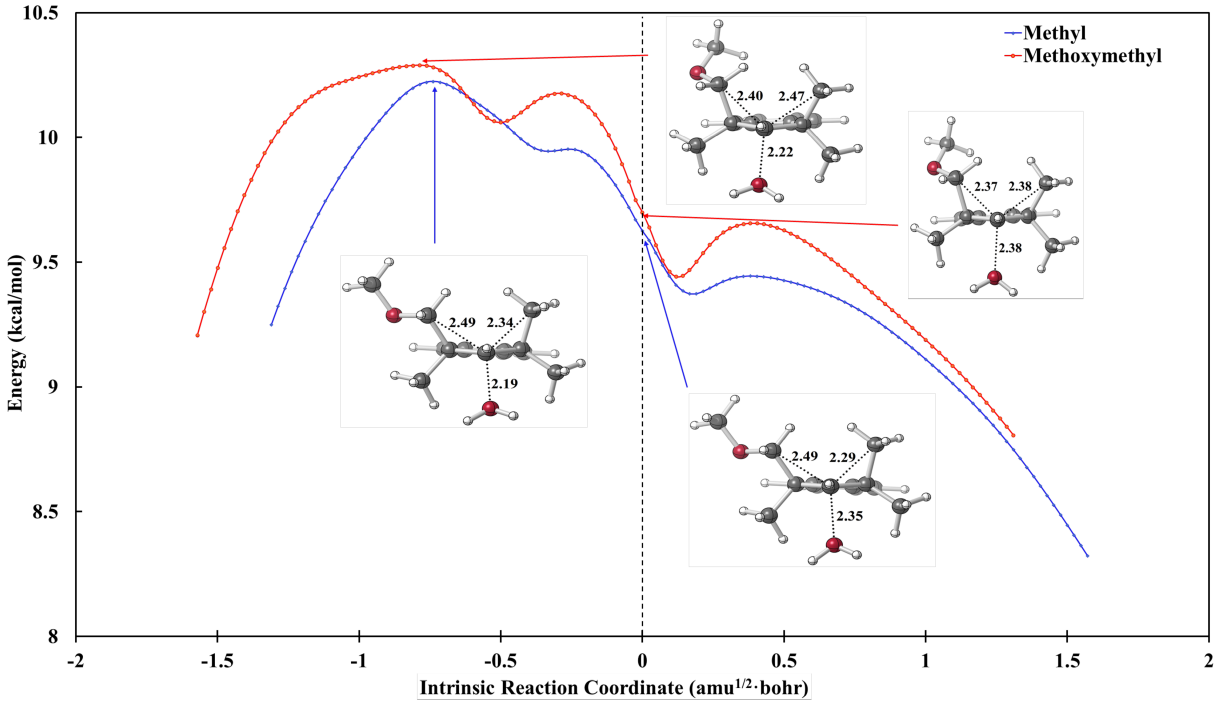

Figure 2. Free energy profiles for the R^1 = methyl, R^2 = methoxymethyl system. Geometries for the conventional TSSs correspond to the '0' point on the horizontal axis. Positions and geometries of VTSs are indicated. In this plot, reactants are on the left-hand side and products are on the right-hand side. See SI for plots with ZPE included but entropy excluded.

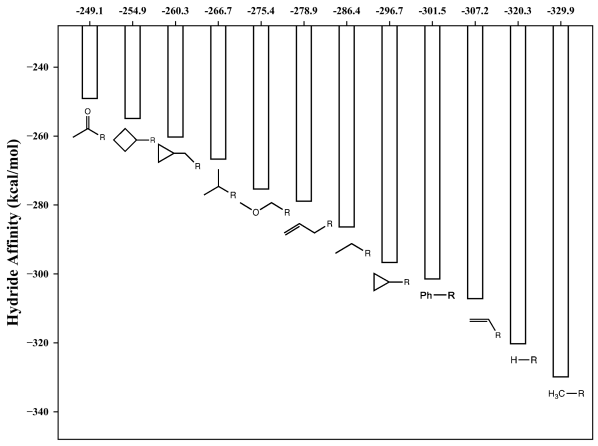

Figure 3. Hydride affinity of selected functional groups. The calculation is performed at M06-2X-D3/def2-TZVPP level of theory. The more negative the enthalpy is, the more thermodynamically unstable the corresponding cation is.

3.4 Hydride affinities of carbocations. Our predicted ordering of migratory aptitudes does not bear out the rule of thumb that better carbocation stabilizers migrate preferentially. One simple approach for quantifying carbocation stabilizing ability is to compare hydride affinities (HA) of cationic forms of the migrating groups—a reasonable approach in that migrating groups generally accumulate positive charge during migration (i.e., TSSs often resemble cations complexed to alkenes).[36] For HAs we use here enthalpies for the reaction of a cation R^+ with H^- to form neutral R–H. Using these values (Figure 5), we arrive at the following order of migratory aptitudes: acyl > cyclobutyl > CH_2-cyclopropyl > *iso*-propyl > methoxymethyl > allyl > ethyl > cyclopropyl > phenyl > vinyl > methyl. Some significant deviations are observed when comparing this ordering to those predicted based on uphill AIMD or transition state energies. For instance, although acyl cation is the most thermodynamically stable cation among all the functional groups tested, it is predicted to be a worse migrator compared with cyclobutyl (Table 1). In addition, the migratory tendencies of the phenyl and cyclobutyl groups are greatly underestimated compared to our dynamics-based predictions (Table 1); while one might imagine that this is a result of stepwise pathways involving phenonium ions or ring-expansion, we find only concerted pathways for our systems. The discrepancies between hydride affinity, statistical kinetic models and dynamic simulations demonstrate the complexity of accurately predicting migratory aptitudes.

3.5 Downhill dynamics and bifurcations. In pursuit of additional insights into the dynamic behavior of our systems, we carried out downhill AIMD simulations for three systems initiated from VTSs (Table 2). Our results reveal several important behaviors. First, a small portion (~5%) of trajectories can access both products, indicating that the two transition states are not completely separated, consistent with the discussion of 2D PESs and similarities of VTS structures above. In other words, either of the two transition states can be viewed as an

ambimodal transition state, although well-defined valley-ridge inflection points are here replaced by a flat portion of

Table 2. Downhill AIMD results with trajectories initiated from VTSs.

TS	R^1	R^2	Recrossing	VTS energy	R^1/R^2 ratio (VTS)[a]	R^1/R^2 ratio (recrossing)[b]	R^1/R^2 ratio (uphill)	Total trajectories
H	47%	5%	48%	9.3	2:98	7:93	30:70	233
cyclopropyl	2%	37%	61%	7.0				321
methyl	63%	3%	34%	10.2	54:46	54:46	86:14	108
methoxymethyl	5%	64%	31%	10.3				121
vinyl	84%	2%	14%	6.8	8:92	7:93	36:64	161
ethyl	47%	0%	53%	8.3				110

a. The R^1/R^2 ratio (VTS) is directly calculated from the Gibbs free energy difference (ΔΔG) of the two VTSs.

b. Recrossing corrections are incorporated into the R^1/R^2 ratio (recrossing) based on the downhill dynamic results, where it is calculated as $\frac{R^1_{VTS1}P_{VTS1}+R^1_{VTS2}P_{VTS2}}{R^2_{VTS1}P_{VTS1}+R^2_{VTS2}P_{VTS2}}$. The subscripts VTS1 and VTS2 indicate the ratio of product 1 or 2 (indicated in superscripts) in the downhill dynamics initiated from the corresponding VTSs. The P_{VTS} indicates the ratio of each VTS based on Boltzmann distribution.

the PES, which allows the minor product to be accessed from the region of the VTS for formation of the major product and vice versa (this cross-over behavior also can be seen in the uphill trajectories mapped onto the surface in Figure 1). The failure of transition state theory to make meaningful predictions when two pathways share one dividing surface is known.[37]

Second, we find a large amount of recrossing, even when initiating trajectories at VTSs. Although transition state theory occupies a central position in the realm of chemical kinetics because it is applicable to most chemical reactions,[23] it is subject to local-equilibrium and non-recrossing assumptions that may become invalid in particular cases.[35,37,38] The non-recrossing assumption states that a trajectory initiated from the reactant region will pass through the dividing surface and advance towards the product region without crossing back through the dividing surface, but deviations from this behavior have been reported. For example, Singleton and co-workers have shown how recrossing can enhance selectivity.[38] Singleton and co-workers also have pointed out that extensive recrossing can serve as a probe for hidden dynamical bottlenecks.[35] Variational transition state theory allows for some recrossing, but a VTS should be associated with minimal recrossing.[37] For some of the cases in Table 2, a large amount of recrossing is observed, up to 61%, despite initiating trajectories at VTSs. Such a high proportion of recrossing trajectories is consistent with a fairly flat surface near the VTS.[8b] The recrossing behavior also is captured in uphill dynamics simulations.

These cross-over and recrossing behaviors are manifested in changes to distances between migrating groups and the carbon that bore the water leaving group during trajectories. In Figure 4 we plot these distances for representative trajectories for a representative reaction (R^1 = cyclopropyl, R^2 = H); the horizontal line across each plot indicates the corresponding C–H distance in the H-migration VTS. In the top panel of Figure 4 are shown trajectories that ultimately form the H-migration product, and it is clear that the C–H distance sometimes dips below and then rises well above the C–H distance in the VTS before dropping to the distance in the product. In addition, the bottom panel of Figure 4, which shows cyclopropyl-migration trajectories, indicates that some of the trajectories sample C–H distances similar to or shorter than those in the region of the VTS for H-migration.

Accounting for cross-over and recrossing observed in downhill AIMD simulations, however, does not change the selectivity predicted using VTS very much. Since we suspect there is a flat surface connecting the two VTSs (in analogy to Figure 1), we expect the product ratio to be sensitive to the position of the starting point for downhill dynamics trajectories, i.e., slightly different C–C or C–H bond distances may lead to drastically different results. To verify this hypothesis, downhill dynamics simulations for **3** (R^1 = cyclopropyl, R^2 = H) were initiated at positions different from the two VTSs (Figure 5). Even though deviations in initial geometries were not large, deviations to product ratios were observed. Specifically, more minor product and, in some cases, less recrossing is observed. Thus it appears that trajectories can roam around the flat inter-transition state region before committing to formation of a particular product (see also Figure 1). Simple VTSs are unable to fully capture the topography of the energy surface.

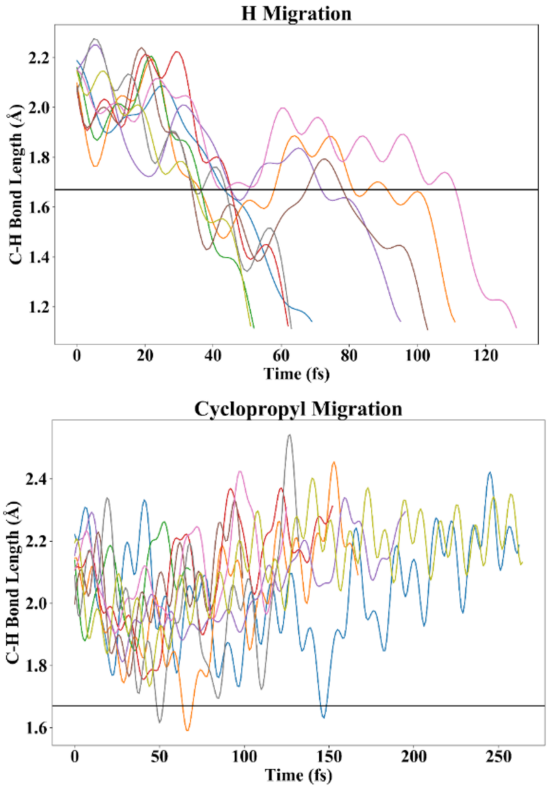

Figure 4. Variations in C–H distances over time for the R^1 = cyclopropyl R^2 = H system. The top panel shows a subset of trajectories that lead to H-migration and the bottom panel shows a subset of trajectories that lead to vinyl-migration. The horizontal black line indicates the C–H distance in the VTS for H-migration.

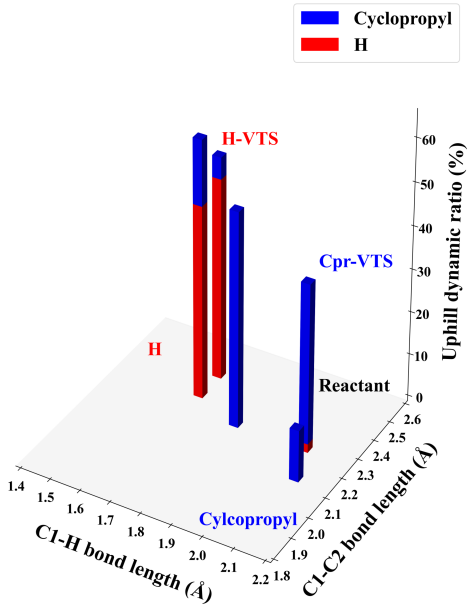

Figure 5. Downhill AIMD simulation results for system **3** (R^1 = cyclopropyl R^2 = H) initiated from different starting points. The colored bars indicate the ratios of products. Blue corresponds to cyclopropyl migration and red corresponds to hydrogen migration. The total height of each bar indicates the total ratio of productive trajectories versus recrossing trajectories. The regions of reactant, cyclopropyl and H migration products are also labeled. All bond lengths are in Å.

3.6 Synthetic relevance. To probe how relevant the approach described above is to actual synthetic and biosynthetic reactions, we investigated a carbocation rearrangement used in Coates and co-workers' biomimetic synthesis of nopsane sesquiterpenes.[25] The synthetic approach involved Wagner-Meerwein rearrangement of a putative secondary carbocation and competition between methyl migration and ring expansion (Scheme 2; secondary carbocation not drawn). The secondary carbocation itself is not a minimum on the PES, and both migrations have their own TSSs – this scenario matches that in our model systems. Here we assume that the experimentally determined product ratio reflects kinetic selectivity for formation of carbocations **24-A** and **24-B**. While we cannot definitively rule out thermodynamic equilibration, in that predicted reverse barriers are only ~12 kcal/mol, we note that the experimentally observed product ratio is not in line with the computed free energy difference for **24-A** and **24-B** and product formation in this case involves trapping by solvent, a process whose rate is difficult to predict accurately.

Firstly, we tested whether predictions using conventional transition state theory match the experimental selectivity. Several levels of theory were examined (see Supporting Information for details) and the highest, DLPNO-CCSD(T)/ def2-QZVPP//M06-2X-D3/def2-TZVP),[39] predicts a Gibbs free energy difference between competing TSSs of 3.3 kcal/mol. This difference implies that no methyl migration product should be observed. However, some methyl migration is observed experimentally, with the observed ratio of products (88:12) corresponding (if transition state theory is employed) to a $\Delta\Delta G^{\ddagger}$ of 1.1 kcal/mol. The discrepancy between theory and experiment is not resolved by employing VTSs (negligible corrections; < 0.2 kcal/mol) or by incorporating implicit solvent ($\Delta\Delta G$ > 2.0 kcal/mol, see Supporting Information for details).

Scheme 2. Carbocation rearrangement in the synthesis of nopsane sesquiterpene.

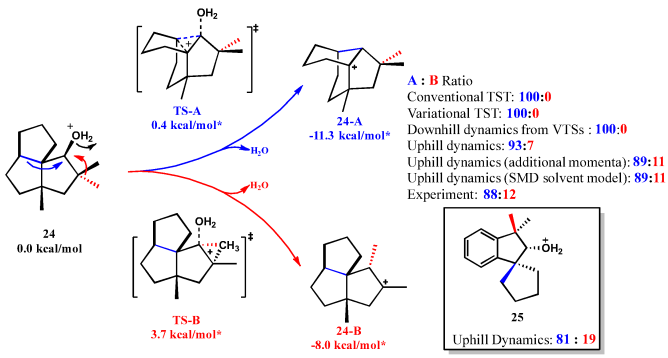

*Free energies at DLPNO-CCSD(T)/def2-QZVPP//M06-2X-D3/def2-TZVP level of theory using tight-PNO.

Might non-statistical dynamic effects be at play here? To investigate this possibility, downhill AIMD simulations were

initiated from the ring-expansion VTS. In the 152 trajectories obtained, no methyl migration was observed. Clearly the presence of a significant amount of the minor product cannot be rationalized by only taking into account non-statistical effects associated with downhill dynamics from the VTSs.

If a flat TS region of the PES spans the two competing transition states as described above, uphill trajectories will not necessarily come near to a VTS. Thus, we again carried out uphill AIMD simulations, here both with and without additional momenta associated with leaving group departure. Additional kinetic energy ranging from 0 to 30 kcal/mol was included in uphill dynamics simulations and a predicted ratio of ~90:10 ratio was found for all the energies (Scheme 2; 365 trajectories with additional momenta; 79 trajectories without additional momenta), consistent with the experimentally observed ratio of 88:12. Additionally, we examined the effect of implicit solvent. Uphill dynamics simulations (118 trajectories) using the SMD model[40] led to a predicted product ratio of 89:11, consistent with the gas phase prediction (see Supporting Information for additional details). This result implies that solvent does not influence the dynamic effects observed for this system, although this contention should be tested with explicit solvent (a goal for our future work).

Could we have predicted this outcome using our model systems alone? Yes. As shown at the bottom right of Scheme 2, competing a cyclopentane ring expansion against a methyl shift in our framework leads to a predicted ratio from uphill AIMD simulations of 81:19, a less accurate but reasonable match.

In summary, the presence of the minor product observed in experiment was not predicted by comparing TSS or VTS free energies or by carrying out downhill AIMD simulations from either. Only uphill AIMD simulations – which allow consequences of a flat inter-transition state region of the PES to be expressed, led to reasonable predictions.

4. Conclusions

We set out to reexamine the concept of migratory aptitude of organic groups from a perspective that includes dynamic effects. While we present here a ranking of migratory aptitudes based on uphill dynamics simulations on model systems designed to capture inherent preferences, the behavior of these model systems turned out to be more complex than expected. This complexity arises in large part from using a molecular framework that allows two migrations to compete with each other. However, this complexity has allowed us to highlight several unusual and/or oft-overlooked behaviors that can influence selectivity. These include momentum effects associated with low barriers and recrossing and inter-transition state roaming associated with the sharing of dividing surfaces by competing transition states.[18,41] While not all experimental systems will have competing transitions states with shared dividing surfaces, it is likely that many will, given the metastability of many carbocations. The examples described here highlight the relevance of such concepts to organic reactions of synthetic and biosynthetic relevance.[14,21a,42]

ASSOCIATED CONTENT

The Supporting Information containing method details, IRCs and coordinates is available free of charge via the Internet at http://pubs.acs.org

AUTHOR INFORMATION

Corresponding Author

***E-mail: djtantillo@ucdavis.edu**

ORCID

Zhitao Feng: 0000-0001-7892-1799

Dean J. Tantillo: 0000-0002-2992-8844

Notes

The authors declare no competing financial interest.

ACKNOWLEDGMENTS

We gratefully acknowledge support from the National Science Foundation (CHE-1856416 and supercomputing resources through a grant from the XSEDE program: CHE-030089). Zhitao Feng also thanks Ruimeng Wang, Zekun Chen, Shunyang Wang, Keming Zhong and Nathaniel J. Troup for insightful suggestions. We also thank Prof. Daniel Singleton for help with energy partitioning analysis.

REFERENCES

1. Fittig, R. Ueber einige Derivate des Acetons. *Justus Liebigs Ann. Chem*. **1860**, *114*, 54–63.
2. Tantillo, D. J. Biosynthesis via carbocations: Theoretical studies on terpene formation. *Nat. Prod. Rep.* **2011**, *28*, 1035-1053.
3. (a) Naredla, R. R.; Klumpp, D. A. Contemporary Carbocation Chemistry: Applications in Organic Synthesis. *Chem. Rev.* **2013**, *113*, 6905-6948 (b) Song, Z.; Fan, C.; Tu, Y. Semipinacol Rearrangement in Natural Product Synthesis. *Chem. Rev*. **2011**, *111*, 7523-7556.
4. (a) Tantillo, D. J. The carbocation continuum in terpene biosynthesis—where are the secondary cations? *Chem. Soc. Rev*. **2010**, *39*, 2847-2854. (b) Hong, Y. J.; Tantillo, D. J. A Maze of Dyotropic Rearrangements and Triple Shifts: Carbocation Rearrangements Connecting Stemarene, Stemodene, Betaerdene, Aphidicolene, and Scopadulanol. *J. Org. Chem.* **2018**, *83*, 3780-3793. (c) Hare, S. R.; Tantillo, D. J. Dynamic behavior of rearranging carbocations–implications for terpene biosynthesis. *Beilstein J. Org. Chem.* **2016**, *12*, 377-390. (d) Bai, M.; Feng, Z.; Li, J.; Tantillo, D. J. Bouncing off walls–widths of exit channels from shallow minima can dominate selectivity control. *Chem. Sci.* **2020**, *11*, 9937-9944.
5. (a) Grob, C. A. Inductivity and bridging in carbocations. *Acc. Chem. Res.* **1983**, *16*, 426-431. (b) Brown, H. C. The energy of the transition states and the intermediate cation in the ionization of 2-norbornyl derivatives. Where is the nonclassical stabilization energy? *Acc. Chem. Res.* **1983**, *16*, 432-440. (c) Olah, G. A.; Prakash, G. K. S.; Saunders, M. Conclusion of the Classical-Nonclassical Ion Controversy Based on the Structural Study of the 2-Norbornyl Cation. *Acc. Chem. Res.* **1983**, *16*, 440-448. (d) Walling, C. An innocent bystander looks at the 2-norbornyl cation. *Acc. Chem. Res.* **1983**, *16*, 448-454. (e) Brown, H. C. (with comments by P. v. R. Schleyer) *The Nonclassical Ion Problem*; Plenum: New York, 1977.

6. (a) Tantillo, D. J. Importance of Inherent Substrate Reactivity in Enzyme- Promoted Carbocation Cyclization/Rearrangements. *Angew. Chem. Int. Ed*. **2017**, *56*, 10040-10045. (b) Ammal, S. C.; Yamataka, H.; Aida, M.; Dupius, M. Dynamics-driven reaction pathway in an intramolecular rearrangement. *Science* **2003**, *299*, 1555-1557. (c) Zhao, C. G.; Feng, Z. T.; Xu, G. Q.; Gao, A.; Chen, J. W.; Wang, Z. Y.; Xu, P. F. Highly Enantioselective Construction of Strained Spiro[2,3]hexanes through a Michael Addition/Ring Expansion/Cyclization Cascade. *Angew. Chem. Int. Ed.* **2020**, *59*, 3058-3062. (d) Carpenter, B. K. Dynamic matching: The cause of inversion of configuration in the [1, 3] sigmatropic migration? *J. Am. Chem. Soc.* **1995**, *117*, 6336-6344.
7. Schreiner, P. R.; Schleyer, P. V.; Schaefer, H. F. Why the Classical and Nonclassical Norbornyl Cations Do Not Resemble the 2-endo- and 2-exo-Norbornyl Solvolysis Transition States. *J. Org. Chem.* **1997**, *62*, 4216-4228.
8. (a) Ess, D. H.; Wheeler, S. E.; Iafe, R. G.; Xu, L.; Çelebi-Ö lçüm, N.; Houk, K. N. Bifurcations on potential energy surfaces of organic reactions. *Angew. Chem., Int. Ed*. **2008**, *47*, 7592−7601. (b) Reis, M. C.; López, C. S.; Faza, O. N.; Tantillo, D. J. Pushing the limits of concertedness. A waltz of wandering carbocations. *Chem. Sci.* **2019**, *10*, 2159-2170. (c) Ghigo, G; Maranzana, A; Tonachini, G. Memory Effects in Carbocation Rearrangements: Structural and Dynamic Study of the Norborn-2-en-7-ylmethyl-X Solvolysis Case. *J. Org. Chem.* **2013**, *78*, 9041-9050.
9. House, H. O.; Grubbs, E. J. The Semipinacolic Deamination of Certain 1-Alkyl-2-amino-1-phenylethanols. *J. Am. Chem. Soc.* **1959**, *81*, 4733–4737.
10. Le Drian, C.; Vogel, P. Facile. Facile migration of acyl groups in Wagner-Meerwein transpositions. Acid-catalyzed rearrangements of 5,6-exo-epoxy-7-oxa-2-bicyclo[2.2.1]heptanone and derivatives. *Tetrahedron Lett.* **1987**, *28*, 1523–1525.
11. Huang, J.; Lebœuf, D.; Frontier, A. J. Understanding the Fate of the Oxyallyl Cation following Nazarov Electrocyclization: Sequential Wagner−Meerwein Migrations and the Synthesis of Spirocyclic Cyclopentenones. *J. Am. Chem. Soc.* **2011**, *133*, 6307–6317.
12. Nakamura, K.; Osamura, Y. Theoretical study of the reaction mechanism and migratory aptitude of the pinacol rearrangement. *J. Am. Chem. Soc.* **1993**, *115*, 9112-9120.
13. de Souza, M. A. F.; Ventura, E.; Monte, S. A. do; Riveros, J. M.; Longo, R. L. Dynamic Effects Dictate the Mechanism and Selectivity of Dehydration–Rearrangement Reactions of Protonated Alcohols [Me2(R)CCH(OH2)Me]+ (R=Me, Et, iPr) in the Gas Phase. *Chem. Eur. J.* **2014**, *20*, 13742–13754.
14. Blumel, M.; Nagasawa, S.; Blackford, K.; Hare, S. R.; Tantillo, D. J.; Sarpong, R. Rearrangement of hydroxylated pinene derivatives to fenchone-type frameworks: computational evidence for dynamically-controlled selectivity. *J. Am. Chem. Soc*. **2018**, *140*, 9291-9298.
15. (a) Wistuba, E.; Rüchardt, C. Intrinsic migration aptitudes of alkyl groups in a pinacol rearrangement. *Tetrahedron Lett.* **1981**, *22*, 4069–4072. (b) Stopka, T.; Schröder, S.; Maulide, N.; Niggemann, M. The Unusual Migratory Aptitude in a Case of α-Carbonyl Cation-Driven 1,2-Migration. *Tetrahedron,* **2020**, *76*, 131460.
16. (a) Liang, T.; Zhang, Z.; Antilla, J. C. Chiral Brønsted acid catalyzed pinacol rearrangement. *Angew. Chem. Int. Ed*. **2010**, *49*, 9734-9736. (b) Snape, T. J. Recent advances in the semi-pinacol rearrangement of α-hydroxy epoxides and related compounds. *Chem. Soc. Rev.* **2006**, *36*, 1823-1842.
17. (a) Hare, S. R.; Pemberton, R. P.; Tantillo, D. J. Navigating past a fork in the road: carbocation− π interactions can manipulate dynamic behavior of reactions facing post-transition-state bifurcations. *J. Am. Chem. Soc*. **2017**, *139*, 7485-7493. (b) Hare, S. R.; Tantillo, D. J. Post-transition state bifurcations gain momentum–current state of the field. *Pure Appl. Chem.* **2017**, *89*, 679-698. (c) Hare, S. R.; Tantillo, D. J. Post-transition state bifurcations induce dynamical detours in Pummerer-like reactions. *Chem. Sci.* **2017**, *8*, 1442-1449. (d) Siebert, M. R.; Manikandan, P.; Sun, R.; Tantillo, D. J.; Hase, W. L. Gas-phase chemical dynamics simulations on the bifurcating pathway of the pimaradienyl cation rearrangement: role of enzymatic steering in abietic acid biosynthesis. *J. Chem. Theory Comput.* **2012**, *8*, 1212−1222. (e) Pemberton, R. P.; Hong, Y. J.; Tantillo, D. J. Inherent dynamical preferences in carbocation rearrangements leading to terpene natural products. *Pure Appl. Chem.* **2013**, *85*, 1949−1957. (f) Hong, Y. J.; Tantillo, D. J. Biosynthetic consequences of multiple sequential post-transition-state bifurcations. *Nat. Chem.* **2014**, *6*, 104−111. (g) Weitman, M.; Major, D. T. Challenges posed to bornyl diphosphate synthase: diverging reaction mechanisms in monoterpenes. *J. Am. Chem. Soc.* **2010**, *132*, 6349− 6360. (h) Lourderaj, U.; Park, K.; Hase, W. L. Classical trajectory simulations of post-transition state dynamics. *Int. Rev. Phys. Chem.* **2008**, *27*, 361–403.
18. (a) Ma, X.; Hase, W. L. Perspective: chemical dynamics simulations of non-statistical reaction dynamics. *Phil. Trans. R. Soc. A* **2017**, *375*, 20160204 (b) Jayee, B.; Hase, W. L. Nonstatistical Reaction Dynamics. *Annu. Rev. Phys. Chem.* **2020**, *71*, 289-313. (c) Carpenter, B. K. Energy disposition in reactive intermediates. *Chem. Rev.* **2013**, *113*, 7265-7286. (d) Barnes, G. L.; Hase, W. L. Direct chemical dynamics simulations. *J. Am. Chem. Soc.* **2017**, *139*, 3570-3590.
19. Campos, R. B.; Tantillo, D. J. Designing Reactions with Post-Transition-State Bifurcations: Asynchronous Nitrene Insertions into C–C σ Bonds. *Chem* **2019**, *5*, 227-236.
20. (a) Pham, H. V.; Houk, K. N. Diels–Alder Reactions of Allene with Benzene and Butadiene: Concerted, Stepwise, and Ambimodal Transition States. *J. Org. Chem.* **2014**, *79*, 8968-8976. (b) Yu, P.; Patel, A.; Houk, K. N. Transannular [6+ 4] and ambimodal cycloaddition in the biosynthesis of heronamide A. *J. Am. Chem. Soc.* **2015**, *137*, 13518-13523.
21. (a) Singleton, D. A.; Hang, C.; Szymanski, M. J.; Greenwald, E. E. A new form of kinetic isotope effect. dynamic effects on isotopic selectivity and regioselectivity. *J. Am. Chem. Soc.* **2003**, *125*, 1176–1177. (b) Carpenter, B. K. Nonstatistical dynamics in thermal reactions of polyatomic molecules. *Annu. Rev. Phys. Chem.* **2005**, *56*, 57–89. (c) Lourderaj, U.; Hase, W. L. Theoretical and computational studies of non-RRKM unimolecular dynamics. *J. Phys. Chem. A*, **2009**, *113*, 2236–2253.
22. Peng, Q.; Paton, R. S. Catalytic control in cyclizations: From computational mechanistic understanding to selectivity prediction. *Acc. Chem. Res.* **2016**, *49*, 1042-1051.
23. (a) Bao, J. L.; Truhlar, D. G. Variational transition state theory: theoretical framework and recent developments. *Chem. Soc. Rev.* **2017**, *46*, 7548-7596. (b) Truhlar, D. G.; Garrett, B. C. Variational transition state theory. *Annu. Rev. Phys. Chem.* **1984**, *35*, 159-189. (c) Garrett, B. C.; Truhlar, D. G. Generalized transition state theory. Classical mechanical theory and applications to collinear reactions of hydrogen molecules. *J. Phy. Chem.* **1979**, *83*, 1052-1079. (d) Garrett, B. C.; Truhlar, D. G.; Grev, R. S.; Magnuson, A. W. Improved treatment of threshold contributions in variational transition-state theory. *J. Phy. Chem.* **1980**, *84*, 1730-1748.
24. (a) Gonzalez, C.; Schlegel, H. B. Reaction path following in mass-weighted internal coordinates. *J. Phys. Chem.* **1990**, *94*, 5523-5527. (b) Fukui, K. The path of chemical reactions-the IRC approach. *Acc. Chem. Res.* **1981**, *14*, 363-368. (c) Maeda, S.; Hara-

buchi, Y.; Ono, Y.; Taketsugu, T.; Morokuma, K. Intrinsic reaction coordinate: Calculation, bifurcation, and automated search. *Int. J. Quantum Chem.* **2015**, *115*, 258-269.

25. Davis, C. E.; Duffy, B. C.; Coates, R. M. Total synthesis of (±)-cameroonan-7α-ol and biomimetic rearrangements to related nopsane sesquiterpenes. *J. Org. Chem*. **2003**, *68*, 6935–6943.
26. Gaussian 16, Revision C.01. Frisch, M. J.; Trucks, G. W.; Schlegel, H. B.; Scuseria, G. E.; Robb, M.A.; Cheeseman, J. R.; Scalmani, G.; Barone, V.; Petersson, G. A.; Nakatsuji, H.; Li, X.; Caricato, M.;Marenich, A. V.; Bloino, J.; Janesko, B. G.; Gomperts, R.; Mennucci, B.; Hratchian, H. P.; Ortiz, J. V.;Izmaylov, A. F.; Sonnenberg, J. L.; Williams-Young, D.; Ding, F.; Lipparini, F.; Egidi, F.; Goings, J.;Peng, B.; Petrone, A.; Henderson, T.; Ranasinghe, D.; Zakrzewski, V. G.; Gao, J.; Rega, N.; Zheng, G.;Liang,W.; Hada, M.; Ehara, M.; Toyota, K.; Fukuda, R.; Hasegawa, J.; Ishida, M.; Nakajima, T.; Honda, Y.; Kitao, O.; Nakai, H.; Vreven, T.; Throssell, K.; Montgomery, J. A., Jr.; Peralta, J. E.; Ogliaro, F.;Bearpark, M. J.; Heyd, J. J.; Brothers, E. N.; Kudin, K. N.; Staroverov, V. N.; Keith, T. A.; Kobayashi,R.; Normand, J.; Raghavachari, K.; Rendell, A. P.; Burant, J. C.; Iyengar, S. S.; Tomasi, J.; Cossi, M.;Millam, J. M.; Klene, M.; Adamo, C.; Cammi, R.; Ochterski, J. W.; Martin, R. L.; Morokuma, K.;Farkas, O.; Foresman, J. B.; Fox, D. J. Gaussian, Inc., Wallingford CT, 2016.
27. Zhao, Y.; Truhlar, D. G. Density functionals with broad applicability in chemistry. *Acc. Chem. Res*. **2008**, *41*, 157-167.
28. Riplinger, C.; Neese, F. An efficient and near linear scaling pair natural orbital based local coupled cluster method. *J. Chem. Phys*. **2013**, *138*, 034106.
29. (a) Neese, F. Software Update: The ORCA Program System,Version 4.0. *Wiley Interdiscip. Rev.: Comput. Mol. Sci.* **2018**, *8*, No. e1327. (b) Neese, F. The ORCA Program System. *Wiley Interdiscip. Rev.: Comput. Mol. Sci.* **2012**, *2*, 73−78.
30. (a) J. Zheng, J. L. Bao, S. Zhang, J. C. Corchado, R. Meana-Pañeda, Y.-Y. Chuang, E. L. Coitiño, B. A. Ellingson, and D. G. Truhlar, *Gaussrate 17*, University of Minnesota, Minneapolis, MN, 2017. (b) J. Zheng, J. L. Bao, R. Meana-Pañeda, S. Zhang, B. J. Lynch, J. C. Corchado, Y.-Y. Chuang, P. L. Fast, W.-P. Hu, Y.-P. Liu, G. C. Lynch, K. A. Nguyen, C. F. Jackels, A. Fernandez Ramos, B. A. Ellingson, V. S. Melissas, J. Villà, I. Rossi, E. L. Coitiño, J. Pu, T. V. Albu, A. Ratkiewicz, R. Steckler, B. C. Garrett, A. D. Isaacson, and D. G. Truhlar, *POLYRATE17*, University of Minnesota, Minneapolis, 2017.
31. Ussing, B. R.; Hang, C.; Singleton, D. A. Dynamic effects on the periselectivity, rate, isotope effects, and mechanism of cycloadditions of ketenes with cyclopentadiene. *J. Am. Chem. Soc*. **2006**, *128*, 7594−7607.
32. Marx, D.; Hutter, J. *Ab initio molecular dynamics: Basic theory and advanced methods*; Cambridge University Press: New York, 2009.
33. Legault, C.Y.; CYLview, 1.0b, Université de Sherbrooke, 2009 (http://www.cylview.org)
34. (a) Chuang, H.-H.; Tantillo, D. J.; Hsu, C.-P. The Construction of Two-Dimensional Potential Energy Surfaces of Reactions with Post-Transition State Bifurcations. *J. Chem. Theory Comput.* **2020**, *16*, 4050-4060. (b) Carpenter, B. K. *Understanding Chemical Reaction Mechanisms, in Of Minds and Molecules, Eds. Nalini Bhushan and Stuart Rosenfeld.* Oxford University Press. New York, 2000, p. 223-224.
35. Gonzalez-James, O. M.; Kwan, E. E.; Singleton, D. A. Entropic intermediates and hidden rate-limiting steps in seemingly concerted cycloadditions. Observation, prediction, and origin of an isotope effect on recrossing. *J. Am. Chem. Soc.* **2012**, *134*, 1914-1917.
36. Cheng, J; Kishan, L. H.; Vernon D. P. Hydride affinities of carbenium ions in acetonitrile and dimethyl sulfoxide solution. *J. Am. Chem. Soc.* **1993**, *115*, 2655-2660.
37. (a) Beno, B. R.; Houk, K. N.; Singleton, D. A. Synchronous or Asynchronous? An "Experimental" Transition State from a Direct Comparison of Experimental and Theoretical Kinetic Isotope Effects for a Diels−Alder Reaction. *J. Am. Chem. Soc.* **1996**, *118*, 9984-9985. (b) Nieves-Quinones, Y.; Singleton, D. A. Dynamics and the regiochemistry of nitration of toluene. *J. Am. Chem. Soc.* **2016**, *138*, 15167-15176. (c) Kurouchi, H.; Sanctis, I. L. A.-D.; Singleton, D. A. Controlling selectivity by controlling energy partitioning in a thermal reaction in solution. *J. Am. Chem. Soc.* **2016**, *138*, 14534-14537 (d) Hase, W. L.; Mondro, S. L.; Duchovic, R. J.; Hirst, D. M. Thermal rate constant for H+ CH3 CH4 recombination. 3. Comparison of experiment and canonical variational transition state theory. *J. Am. Chem. Soc.* **1987**, *109*, 2916-2922. (e) Pradhan, R.; Lourderaj, U. Can reactions follow non-traditional second-order saddle pathways avoiding transition states? *Phys. Chem. Chem. Phys.* **2019**, *21*, 12837-12842.
38. Wang, Z.; Hirschi, J. S.; Singleton, D. A. Recrossing and dynamic matching effects on selectivity in a Diels–Alder reaction. *Angew. Chem. Int. Ed*. **2009**, *48*, 9156-9159.
39. Weigend, F.; Ahlrichs, R. Balanced basis sets of split valence, triple zeta valence and quadruple zeta valence quality for H to Rn: Design and assessment of accuracy. *Phys. Chem. Chem. Phys*. **2005**, *7*, 3297-3305.
40. Marenich, A. V.; Cramer, C. J.; Truhlar, D. G. Universal solvation model based on solute electron density and on a continuum model of the solvent defined by the bulk dielectric constant and atomic surface tensions. *J. Phys. Chem. B.* **2009,** *18*, 6378-6396.
41. Townsend, D.; Lahankar, S. A.; Lee, S. K.; Chambreau, S. D.; Suits, A. G.; Zhang, X.; Rheinecker, J.; Harding, L. B.; Bowman, J. M. The roaming atom: straying from the reaction path in formaldehyde decomposition. *Science* **2004**, *306*, 1158-1161.
42. (a) Laconsay, C. J.; Tsui, K. Y.; Tantillo, D. J. Tipping the balance: theoretical interrogation of divergent extended heterolytic fragmentations. *Chem. Sci.* **2020**, *11*, 2231-2242. (b) Xu, L.; Doubleday, C. E.; Houk, K. N. Dynamics of carbene cycloadditions. *J. Am. Chem. Soc*. **2011**, *133*, 17848-17854. (c) Bailey, J. O.; Singleton, D. A. Failure and redemption of statistical and nonstatistical rate theories in the hydroboration of alkenes. *J. Am. Chem. Soc.* **2017**, *139*, 15710-15723.

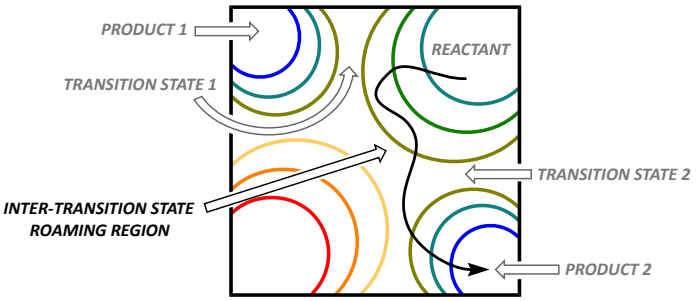
PRODUCT 1
REACTANT
TRANSITION STATE 1
TRANSITION STATE 2
INTER-TRANSITION STATE
ROAMING REGION
PRODUCT 2